Inorg. Chem. **2006**, *45*, 8942–8949

Synthesis, Crystal Structures, and Magnetic Properties of Cyano-Bridged Heterobimetallic Chains Based on $[(Tp)Fe(CN)_3]^-$

He-Rui Wen,[†] Cai-Feng Wang,[†] You Song,[†] Song Gao,[‡] Jing-Lin Zuo,*[,†] and Xiao-Zeng You[†]

Coordination Chemistry Institute, State Key Laboratory of Coordination Chemistry, Nanjing University, Nanjing 210093, China, and State Key Laboratory of Rare Earth Materials Chemistry and Applications, College of Chemistry and Molecular Engineering, Peking University, Beijing 100871, China

Received May 28, 2006

With the use of the tailored cyanometalate precursor, $(Bu_4N)[(Tp)Fe(CN)_3]$ (Tp = Tris(pyrazolyl)hydroborate) as the building block to react with fully solvated Cu^{II}, Co^{II}, and Ni^{II} cations, four one-dimensional (1D) heterobimetallic cyano-bridged chain complexes of squares, $[(Tp)_2Fe^{III}{}_2(CN)_6Cu(CH_3OH)\cdot 2CH_3OH]_n$ (**1**), $[(Tp)_2Fe^{III}{}_2(CN)_6Cu(DMF)\cdot DMF]_n$ (**2**), $[(Tp)_2Fe^{III}{}_2(CN)_6M(CH_3OH)_2\cdot 2CH_3OH]_n$ (M = Co (**3**) and Ni (**4**)), have been prepared. In complexes **1** and **2**, the Cu^{II} ions are pentacoordinated in the form of a slightly distorted square-based pyramid, and they are linked by distorted octahedrons of $[(Tp)Fe(CN)_3]^-$ to form 1D chains of squares. In complexes **3** and **4**, both the central Co^{II} and Ni^{II} ions have a slightly distorted octahedral coordination geometry, and they are bridged by $[(Tp)Fe(CN)_3]^-$ to form similar 1D chains of squares. There are weak interchain π–π stacking interactions through the pyrazolyl groups of the Tp ligands for complexes **3** and **4**. The crystal structures and magnetic studies demonstrate that complexes **1** and **2** exhibit intrachain ferromagnetic coupling and single-chain magnets behavior, and the blocking temperature is ca. 6 K for complex **1** and ca. 3 K for complex **2**. Complexes **3** and **4** show significant metamagnetic behavior, where the cyanides mediate the intrachain ferromagnetic coupling between Fe^{III} and Co^{II} or Ni^{II} ions and the interchain π–π stacking interactions lead to antiferromagnetic couplings. The field dependence of the magnetization measurements shows that the critical field is around 1 kOe for complex **3** and 0.8 kOe for complex **4** at 1.8 K.

Introduction

The discovery of single-molecule magnets (SMMs) enables the storage of information at the molecular and nanoscale level, which may be used in molecular devices and quantum computer science.[1] Recently, one-dimensional (1D) chain compounds named either magnetic nanowires or single-chain magnets (SCMs) have attracted increasing interest because they exhibit the same slow magnetic relaxation as the single-molecule magnets but with possible high magnetic transition temperature.[2]

Because of its convenience to direct the formation of structure and efficiency to transfer the magnetic interaction,[3] cyanide becomes a fascinating bridging ligand in the research for magnetic materials such as high-T_c magnets,[4] spin crossover materials,[5] and single-molecule[6] and single-chain magnets.[7] Recently, the approach of introduction of capping ligands as blocking groups into metal−cyanide systems to

* To whom correspondence should be addressed. E-mail: zuojl@nju.edu.cn. Fax: +86-25-83314502.

[†] Coordination Chemistry Institute.

[‡] State Key Laboratory of Rare Earth Materials Chemistry and Applications.

(1) (a) Wernsdorfer, W.; Sessoli, R. *Science* **1999**, *284*, 133−135. (b) Leuenberger, M. N.; Loss, D. *Nature* **2001**, *410*, 789−793.

(2) (a) Caneschi, A.; Gatteschi, D.; Lalioti, N.; Sangregorio, C.; Sessoli, R.; Venturi, G.; Vindigni, A.; Rettori, A.; Pini, M. G.; Novak, M. A. *Angew. Chem., Int. Ed.* **2001**, *40*, 1760−1763. (b) Clérac, R.; Miyasaka, H.; Yamashita, M.; Coulon, C. *J. Am. Chem. Soc.* **2002**, *124*, 12837−12844. (c) Liu, T.-F.; Fu, D.; Gao, S.; Zhang, Y.-Z.; Sun, H.-L.; Su, G.; Liu, Y.-J. *J. Am. Chem. Soc.* **2003**, *125*, 13976−13977. (d) Ferbinteanu, M.; Miyasaka, H.; Wernsdorfer, W.; Nakata, K.; Sugiura, K.-I.; Yamashita, M.; Coulon, C.; Clérac, R. *J. Am. Chem. Soc.* **2005**, *127*, 3090−3099. (e) Kajiwara, T.; Nakano, M.; Kaneko, Y.; Takaishi, S.; Ito, T.; Yamashita, M.; Igashira-Kamiyama, A.; Nojiri, H.; Ono, Y.; Kojima, N. *J. Am. Chem. Soc.* **2005**, *127*, 10150−10151. (f) Bogani, L.; Sangregorio, C.; Sessoli, R.; Gatteschi, D. *Angew. Chem., Int. Ed.* **2005**, *44*, 5817−5821.

(3) (a) Dunbar, K. R.; Heintz, R. A. *Prog. Inorg. Chem.* **1997**, *45*, 283−391. (b) Weihe, H.; Güdel, H. U. *Comments Inorg. Chem.* **2000**, *22*, 75−103. (c) Miller, J. S. *MRS Bull.* **2000**, *25*, 60−64. (d) Marvaud, V.; Decroix, C.; Scuiller, A.; Guyard-Duhayon, C.; Vaissermann, J.; Gonnet, F.; Verdaguer, M. *Chem. Eur. J.* **2003**, *9*, 1677−1691.

10.1021/ic060928d CCC: $33.50
Published on Web 09/29/2006

preclude the formation of multidimensional arrays has been developed. If the transition metal ions toward hexacyanometalates are partially blocked with polydentate ligands, some interesting lower-dimensional heterobimetallic compounds with different topologies and structures have been obtained.[3d,6b,c,8] An alternative synthetic strategy is to use building blocks of modified cyanometalates $[M(L)_y(CN)_x]^{(x-m)-}$ where L is an organic polydentate ligand, such as phen, bipy,[9] tacn and its derivatives,[10] tach,[11] Cp,[12] bpca,[13] or Tp and its derivatives.[14] On the basis of these building blocks, some heterobimetallic complexes exhibiting interesting magnetic properties were synthesized,[10−15] including single-molecule magnets[6a,f−j] and single-chain magnets.[7]

Up to now, it has been difficult to predict and fulfill experimentally the requirements of a perfect 1D Ising-type chain. The enhancement of the steric effect to decrease the interchain interaction and introduction of anisotropic elements to tune the magnetic exchange are expected to play an important role in the formation of single-chain magnets. The tailored cyanometalate precursor, $[(Tp)Fe^{III}(CN)_3]^-$ (Tp = Tris(pyrazolyl)hydroborate), has been chosen as our main building block. In comparison to those precursors reported before,[9−11] $[(Tp)Fe^{III}(CN)_3]^-$ is sterically more demanding and bears a negative charge. Herein, we report the syntheses, crystal structures, and magnetic properties of four 1D cyano-bridged heterobimetallic chain complexes, $[(Tp)_2Fe_2^{III}(CN)_6Cu(CH_3OH)\cdot 2CH_3OH]_n$ (**1**), $[(Tp)_2Fe_2^{III}(CN)_6Cu(DMF)\cdot DMF]_n$ (**2**), $[(Tp)_2Fe^{III}{}_2(CN)_6M(CH_3OH)_2\cdot 2CH_3OH]_n$ (M = Co (**3**) and Ni (**4**)). Complex **1** exhibits single-chain magnet behavior and has been briefly reported in a preliminary communication.[7c] With the same structure, the solvated and coordinated methanol molecules in complex **1** are replaced by more bulky solvent molecules (DMF) in **2**, which also shows the slow relaxation like SCMs. Complexes **3** and **4** are 1D coordination polymers with metamagnetic behavior.

Experimental Section

Materials and Physical Measurements. All chemicals and solvents used during the synthesis were reagent grade and used as received. $(Bu_4N)[(Tp)Fe(CN)_3]$ was synthesized as described in the literature method.[14a] Elemental analyses for C, H, and N were performed on a Perkin-Elmer 240C analyzer. Infrared spectra were recorded on a Vector22 Bruker spectrophotometer with KBr pellets in the 400−4000 cm^{-1} region.

Caution: Cyanides are very toxic and should be handled with great caution.

Preparation of $[(Tp)_2Fe^{III}{}_2(CN)_6Cu(CH_3OH)\cdot 2CH_3OH]_n$ (1). A mixture of methanol and water (v/v 1:1, 2 mL) was gently layered

(4) (a) Ferlay, S.; Mallah, T.; Quahès, R.; Veillet, P.; Verdaguer, M. *Nature* **1995**, *378*, 701−703. (b) Sato, O.; Iyoda, T.; Fujishima, A.; Hashimoto, K. *Science* **1996**, *271*, 49−51. (c) Holmes, S. M.; Girolami, G. S. *J. Am. Chem. Soc.* **1999**, *121*, 5593−5594. (d) Hatlevik, Ø.; Buschman, W. E.; Zhang, J.; Manson, J. L.; Miller, J. S. *Adv. Mater.* **1999**, *11*, 914−918.

(5) (a) Niel, V.; Thompson, A. L.; Muñoz, M. C.; Galet, A.; Goeta, A. E.; Real, J. A. *Angew. Chem., Int. Ed.* **2003**, *42*, 3760−3763. (b) Molnár, G.; Niel, V.; Gaspar, A. B.; Real, J. A.; Zwick, A.; Bousseksou, A.; McGarvey, J. J. *J. Phys. Chem. B* **2002**, *106*, 9701−9707. (c) Molnár, G.; Niel, V.; Real, J. A.; Dubrovinsky, L.; Bousseksou, A.; McGarvey, J. J. *J. Phys. Chem. B* **2003**, *107*, 3149−3155.

(6) (a) Sokol, J. J.; Hee, A. G.; Long, J. R. *J. Am. Chem. Soc.* **2002**, *124*, 7656−7657. (b) Berlinguette, C. P.; Vaughn, D.; Cañada-Vilalta, C.; Galán-Mascarós, J. R.; Dunbar, K. R. *Angew. Chem., Int. Ed.* **2003**, *42*, 1523−1526. (c) Mironov, V. S.; Chibotaru, L. F.; Ceulemans, A. *J. Am. Chem. Soc.* **2003**, *125*, 9750−9760. (d) Choi, H. J.; Sokol, J. J.; Long, J. R. *Inorg. Chem.* **2004**, *43*, 1606−1608. (e) Schelter, E. J.; Prosvirin, A. V.; Dunbar, K. R. *J. Am. Chem. Soc.* **2004**, *126*, 15004−15005. (f) Wang, S.; Zuo, J. L.; Zhou, H. C.; Choi, H. J.; Ke, Y.; Long, J. R.; You, X. Z. *Angew. Chem., Int. Ed.* **2004**, *43*, 5940−5943. (g) Li, D.; Parkin, S.; Wang, G.; Yee, G. T.; Prosvirin, A. V.; Holmes, S. M. *Inorg. Chem.* **2005**, *44*, 4903−4905. (h) Ni, Z. H.; Kou, H. Z.; Zhang, L. F.; Ge, C.; Cui, A. L.; Wang, R. J.; Li, Y.; Sato O. *Angew. Chem., Int. Ed.* **2005**, *44*, 7742−7745. (i) Li, D.; Parkin, S.; Wang, G.; Yee, G. T.; Clérac, R.; Wernsdorfer, W.; Holmes S. M. *J. Am. Chem. Soc.*, **2006**, *128*, 4214−4215. (j) Wang, C. F.; Zuo, J. L.; Bartlett, B. M.; Song, Y.; Long, J. R.; You, X. Z. *J. Am. Chem. Soc.* **2006**, *128*, 7162−7163.

(7) (a) Lescouëzec, R.; Vaissermann, J.; Ruiz-Pérez, C.; Lloret, F.; Carrasco, R.; Julve, M.; Verdaguer, M.; Dromzee, Y.; Gatteschi, D.; Wernsdorfer, W. *Angew. Chem., Int. Ed.* **2003**, *42*, 1483−1486. (b) Toma, L. M.; Lescouëzec, R.; Lloret, F.; Julve, M.; Vaissermann, J.; Verdaguer, M. *Chem. Commun.* **2003**, 1850−1851. (c) Wang, S.; Zuo, J.-L.; Gao, S.; Song, Y.; Zhou, H.-C.; Zhang, Y.-Z. *J. Am. Chem. Soc.* **2004**, *126*, 8900−8901. (d) Toma, L. M.; Lescouëzec, R.; Pasán, J.; Ruiz-Pérez, C.; Vaissermann, J.; Cano, J.; Carrasco, R.; Wernsdorfer, W.; Lloret, F.; Julve, M. *J. Am. Chem.* Soc., **2006**, *128*, 4842−4853.

(8) (a) Colacio, E.; Domínguez-Vera, J. M.; Ghazi, M.; Kivekäs, R.; Klinga, M.; Moreno, J. M. *Chem. Commun.* **1998**, 1071−1072. (b) Miyasaka, H.; Ieda, H.; Matsumoto, N.; Re, N.; Crescenzi, R.; Floriani, C. *Inorg. Chem.* **1998**, *37*, 255−263. (c) Ohba, M.; Ôkawa, H. *Coord. Chem. Rev.* **2000**, *198*, 313−328. (d) Parker, R. J.; Spiccia, L.; Berry, K. J.; Fallon, G. D.; Moubaraki, B.; Murray, K. S. *Chem. Commun.* **2001**, 333−334. (e) EI Fallah, M. S.; Ribas, J.; Solans, X.; Font-Bardia, M. *J. Chem. Soc. Dalton Trans.* **2001**, 247−250. (f) Černák, J.; Orendáč, M.; Potočňák, I.; Chomič, J.; Orendáčová, A.; Skoršepa, J.; Feher, A. *Coord. Chem. Rev.* **2002**, *224*, 51−66. (g) Marvaud, V.; Decroix, C.; Scuiller, A.; Tuyèras, F.; Guyard-Duhayon, C.; Vaissermann, J.; Marrot, J.; Gonnet, F.; Verdaguer, M. *Chem. Eur. J.* **2003**, *9*, 1692−1705.

(9) (a) Lescouëzec, R.; Lloret, F.; Julve, M.; Vaissermann, J.; Verdaguer, M.; Llusar, R.; Uriel, S. *Inorg. Chem.* **2001**, *40*, 2065−2072. (b) Lescouëzec, R.; Lloret, F.; Julve, M.; Vaissermann, J.; Verdaguer, M. *Inorg. Chem.* **2002**, *41*, 818−826. (c) Toma, L.; Lescouëzec, R.; Vaissermann, J.; Delgado, F. S.; Ruiz-pérez, C.; Carrasco, R.; Cano, J.; Lloret, F.; Julve, M. *Chem. Eur. J.* **2004**, *10*, 6130−6145. (d) Toma, L. M.; Delgado, F. S.; Ruiz-Pérez, C.; Carrasco, R.; Cano, J.; Lloret, F.; Julve, M. *J. Chem. Soc., Dalton Trans.* **2004**, 2836−2846. (e) Zhang, Y. Z.; Gao, S.; Wang, Z. M.; Su, G.; Sun, H. L.; Pan, F. *Inorg. Chem.* **2005**, *44*, 4534−4545. (f) Toma, L.; Toma, L. M.; Lescouëzec, R.; Armentano, D.; Munno, G. D.; Andruh, M.; Cano, J.; Lloret, F.; Julve, M. *J. Chem. Soc., Dalton Trans.* **2005**, 1357−1364.

(10) (a) Heinrich, J. L.; Berseth, P. A.; Long, J. R. *Chem. Commun.* **1998**, 1231−1232. (b) Berseth, P. A.; Sokol, J. J.; Shores, M. P.; Heinrich, J. L.; Long, J. R. *J. Am. Chem. Soc.* **2000**, *122*, 9655−9662. (c) Shores, M. P.; Sokol, J. J.; Long, J. R. *J. Am. Chem. Soc.* **2002**, *124*, 2279−2292. (d) Yang, J. Y.; Shores, M. P.; Sokol, J. J.; Long, J. R. *Inorg. Chem.* **2003**, *42*, 1403−1419. (e) Rebilly, J. N.; Catala, L.; Rivière, E.; Guillot, R.; Wernsdorfer, W.; Mallah, T. *Inorg. Chem.* **2005**, *44*, 8194−8196.

(11) Sokol, J. J.; Shores, M. P.; Long, J. R. *Angew. Chem., Int. Ed.* **2001**, *40*, 236−239.

(12) (a) Klausmeyer, K. K.; Rauchfuss, T. B.; Wilson, S. R. *Angew. Chem., Int. Ed.* **1998**, *37*, 1694−1696. (b) Klausmeyer, K. K.; Wilson, S. R.; Rauchfuss, T. B. *J. Am. Chem. Soc.* **1999**, *121*, 2705−2711. (c) Contakes, S. M.; Klausmeyer, K. K.; Rauchfuss, T. B. *Inorg. Chem.* **2000**, *39*, 2069−2075. (d) Darensbourg, D. J.; Lee, W. Z.; Adams, M. J.; Yarbrough, J. C. *Eur. J. Inorg. Chem.* **2001**, 2811−2822.

(13) (a) Lescouëzec, R.; Vaissermann, J.; Toma, L. M.; Carrasco, R.; Lloret, F.; Julve, M. *Inorg. Chem.* **2004**, *43*, 2234−2236. (b) Wen, H. R.; Wang, C. F.; Zuo, J. L.; Song, Y.; Zeng, X. R.; You, X. Z. *Inorg. Chem.* **2006**, *45*, 582−590.

(14) (a) Lescouëzec, R.; Vaissermann, J.; Lloret, F.; Julve, M.; Verdaguer, M. *Inorg. Chem.* **2002**, *41*, 5943−5945. (b) Wang, S.; Zuo, J. L.; Zhou, H. C.; Song, Y.; Gao, S.; You, X. Z. *Eur. J. Inorg. Chem.* **2004**, 3681−3687. (c) Li, D.; Parkin, S.; Wang, G.; Yee, G. T.; Prosvirin, A. V.; Holmes, S. M. *Inorg. Chem.* **2006**, *45*, 1951−1959.

(15) (a) Lescouëzec, R. L.; Toma, L. M.; Vaissermann, J.; Verdaguer, M.; Delgado, F. S.; Ruiz-Pérez, C.; Lloret, F.; Julve, M. *Coord. Chem. Rev.* **2005**, *249*, 2691−2729 and references therein. (b) Beltran, L. M. C.; Long, J. R. *Acc. Chem. Res.* **2005**, *38*, 325−334.

Table 1. Summary of Crystallographic Data for the Complexes **1**, **2**, **3**, and **4**

	1	**2**	**3**	**4**
formula	$C_{27}H_{32}B_2CuFe_2N_{18}O_3$	$C_{30}H_{34}B_2CuFe_2N_{20}O_2$	$C_{28}H_{36}B_2CoFe_2N_{18}O_4$	$C_{28}H_{36}B_2Fe_2N_{18}NiO_4$
fw	853.57	903.63	881.00	880.78
crystal system	monoclinic	monoclinic	monoclinic	monoclinic
space group	$P2_1/c$	$P2_1/c$	$C2/c$	$C2/c$
a, Å	15.0248(9)	15.249(3)	27.6489(9)	27.427(3)
b, Å	19.0019(12)	20.201(4)	11.5053(4)	11.3692(11)
c, Å	13.4159(8)	13.488(2)	13.1287(5)	13.0941(14)
α, deg	90	90	90	90
β, deg	100.55(10)	99.509(3)	102.525(2)	102.767(4)
γ, deg	90	90	90	90
V, Å^3	3765.4(4)	4097.5(12)	4077.0(2)	3982.1(7)
Z	4	4	4	4
D_{calcd}, g cm^{-3}	1.506	1.465	1.435	1.469
T/K	213	293(2)	293(2)	293(2)
μ, mm^{-1}	1.376	1.269	1.161	1.245
F(000)	1740	1844	1804	1808
index ranges	$-17 \le h \le 17$	$-18 \le h \le 18$	$-37 \le h \le 38$	$-33 \le h \le 32$
	$-22 \le k \le 17$	$-24 \le k \le 23$	$-16 \le k \le 16$	$-10 \le k \le 14$
	$-15 \le l \le 15$	$-16 \le l \le 16$	$-18 \le l \le 18$	$-14 \le l \le 16$
data/restraints/parameters	6620/0/498	8022/0/518	6152/0/264	3908/0/251
GOF (F^2)	1.012	1.036	1.083	1.003
R1, wR2 ($I > 2\sigma(I)$)	0.0407, 0.0988	0.0546, 0.1113	0.0310, 0.0844	0.0452, 0.1122
R1[a], wR2[b] (all data)	0.0596, 0.1084	0.0824, 0.1169	0.0485, 0.0890	0.0591, 0.1160

on top of a solution of $Cu(NO_3)_2 \cdot 6H_2O$ (15 mg, 0.05 mmol) in 2 mL of water. A solution of $(Bu_4N)[(Tp)Fe(CN)_3]$ (59 mg, 0.1 mmol) in 2 mL of methanol was added carefully as a third layer. Brown needlelike crystals of **1** were obtained after 2 weeks. Yield: 80%. Anal. Calcd for $C_{27}H_{32}B_2CuFe_2N_{18}O_3$: C, 38.02; H, 3.44; N, 30.69. Found: C, 37.86; H, 3.53; N, 30.31. IR (KBr): ν(B−H) 2516 cm^{-1}; ν(C≡N) 2177 and 2129 cm^{-1}.

$[(Tp)_2Fe^{III}_2(CN)_6Cu(DMF)\cdot DMF]_n$ (2). A solution of $Cu(NO_3)_2 \cdot 6H_2O$ (7.4 mg, 0.025 mmol) in 1 mL of DMF was added to the solution of $(Bu_4N)[(Tp)Fe^{III}(CN)_3]$ (29 mg, 0.05 mmol) in 1 mL of DMF. Brown-red needlelike crystals of complex **2** were obtained by slow diffusion of diethyl ether into the resulting solution. Yield: 53%. Anal. Calcd for $C_{30}H_{34}B_2CuFe_2N_{20}O_2$: C, 51.28; H, 4.52; N, 28.15. Found: C, 51.29; H, 4.54; N, 27.79. IR (KBr): ν(B−H) 2519 cm^{-1}; ν(C≡N) 2176 and 2129 cm^{-1}; ν(C═O) 1678 and 1653 cm^{-1}.

$[(Tp)_2Fe^{III}_2(CN)_6Co(CH_3OH)_2\cdot 2CH_3OH]_n$ (3). A solution of $(Bu_4N)[(Tp)Fe(CN)_3]$ (59 mg, 0.1 mmol) in 20 mL of methanol was added to a solution of $Co(NO_3)_2 \cdot 6H_2O$ (15 mg, 0.05 mmol) in 5 mL of water. Slow evaporation of the resulting solution in air resulted to the formation of red crystals after 1 week. Yield: 63%. Anal.Calcd for $C_{28}H_{36}B_2CoFe_2N_{18}O_4$: C, 42.51; H, 2.72; N, 19.84. Found: C, 42.45; H, 2.57; N, 19.68. IR (KBr): ν(B−H) 2513 cm^{-1}; ν(C≡N) 2160 and 2124 cm^{-1}.

$[(Tp)_2Fe^{III}_2(CN)_6Ni(CH_3OH)_2\cdot 2CH_3OH]_n$ (4). A solution of $Ni(ClO_4)_2 \cdot 6H_2O$ (18 mg, 0.05 mmol) in 3 mL of water was added to a solution of $(Bu_4N)[(Tp)Fe(CN)_3]$ (59 mg, 0.1 mmol) in 12 mL of methanol. After slow evaporation of the resulting solution in air, orange-red crystals were obtained after 2 weeks. Yield: 72%. Anal. Calcd for $C_{28}H_{36}B_2Fe_2N_{18}NiO_4$: C, 38.15; H, 3.97; N, 28.61. Found: C, 38.45; H, 3.76; N, 28.93. IR (KBr): ν(B−H) 2514 cm^{-1}; ν(C≡N) 2166 and 2123 cm^{-1}.

X-ray Structure Determination. The crystal structures were determined on a Bruker SMART APEX CCD diffractometer using monochromated Mo Kα radiation (λ = 0.71073 Å) at room temperature. Cell parameters were retrieved using SMART software and refined using SAINT on all observed reflections. Data were collected using a narrow-frame method with scan widths of 0.30° in ω and an exposure time of 10 s/frame. The highly redundant data sets were reduced using SAINT and corrected for Lorentz and polarization effects. Absorption corrections were applied using SADABS supplied by Bruker. Structures were solved by direct methods using the program SHELXL-97. The positions of metal atoms and their first coordination spheres were located from direct methods *E*-maps; other non-hydrogen atoms were found in alternating difference Fourier syntheses and least-squares refinement cycles and, during the final cycles, refined anisotropically. Hydrogen atoms were placed in calculated position and refined as riding atoms with a uniform value of U_{iso}. Final crystallographic data and values of R1 and wR are listed in Table 1.

Magnetic Susceptibility Measurements. Magnetic susceptibility measurements for all crystalline samples were obtained with the use of a Quantum Design MPMS-XL7 SQUID magnetometer at temperatures ranging from 1.8 to 300 K. The dc measurements were collected from −70 to 70 kOe. Data were corrected for the diamagnetic contribution calculated from Pascal constants. The ac measurements were performed at various frequencies from 1 to 1500 Hz with the ac field amplitude of 5 Oe and no dc field applied.

Results and Discussion

Syntheses. The anionic precursor $[(Tp)Fe(CN)_3]^-$ has been chosen as the building block to prepare cyano-bridged multinuclear clusters and coordination polymers. The tetrabutylammonium salt of $[(Tp)Fe(CN)_3]^-$ was prepared in good yield (78%). It is soluble in most organic solvents such as acetonitrile, acetone, methanol, and DMF. The paramagnetic result of magnetic measurements and the cyanide stretching frequency at 2117 cm^{-1} demonstrate the low-spin character of the iron(III) in $[(Tp)Fe(CN)_3]^-$.

Reaction of $Cu(ClO_4)_2 \cdot 6H_2O$ with $(Bu_4N)[(Tp)Fe^{III}(CN)_3]$ in acetonitrile and ethanol (mole ratio = 2:1) yielded the isolation of a face-centered cubic cluster, $[(Tp)_8(H_2O)_6Cu^{II}_6Fe^{III}_8(CN)_{24}]^{4+}$, showing single-molecule magnet behavior with a well-isolated $S = 7$ ground state.[6f] This 14-metal cluster is soluble in DMF or acetonitrile. The C≡N stretching region in the infrared spectrum of this cluster (a peak of medium intensity at 2176 cm^{-1}) is consistent with the presence of only bridging cyanide ligands and the high symmetry of the structure. The reaction of $Cu(NO_3)_2 \cdot 6H_2O$ and $(Bu_4N)[(Tp)Fe(CN)_3]$ in methanol and water led to the

Table 2. Selected Bond Lengths (Å) and Angles (deg) for Complexes **1** and **2**[a]

	1	**2**
Cu−N	1.968(3), 1.952(3)	1.946(3), 1.977(3)
	1.965(3), 1.988(3)	1.980(3), 1.990(3)
Cu−O	2.232(3)	2.181(3)
Fe−CN	1.911(3) 1.920(4), 1.933(4)	1.898(5), 1.909(4), 1.926(4)
Fe−N_{pz}	1.960(3), 1.963(3), 1.967(3)	1.961(3), 1.975(3), 1.986(3)
C−N_{cyano}	1.143(4), 1.145(4), 1.146(4)	1.155(5), 1.143(5), 1.132(5)
Fe−C−N	174.5(3), 175.4(3)	175.2(3), 179.7(4)
	175.3(3), 175.9(4)	177.9(4), 178.0(4)
Cu−N−C	167.4(3), 173.4(3)	175.9(4), 168.0(3)
	176.2(3), 179.3(3)	170.1(3), 170.4(3)
N−Cu−N	87.11(12), 90.77(12)	89.94(13), 91.17(13)
	88.98(11), 90.80(11)	88.65(13), 88.41(13)

[a] N_{cyano}, N_{pz} indicate N atoms in cyanide and in pyrazolyl ligands, respectively.

formation of the 1D polymeric complex, $[(Tp)_2Fe_2^{III}(CN)_6Cu(CH_3OH)\cdot 2CH_3OH]_n$ (**1**). The reaction is driven by the formation of the insoluble neutral polymer. Two C≡N stretching vibrations are observed at 2129 and 2177 cm^{-1}, and this is consistent with the presence of bridging and terminal cyanide ligands. When complex **1** is gradually dissolved in DMF or from the reaction of $Cu(NO_3)_2\cdot 6H_2O$ and $(Bu_4N)[(Tp)Fe(CN)_3]$ in DMF, the DMF solvated analogue of **1**, $[(Tp)_2Fe^{III}_2(CN)_6Cu(DMF)\cdot DMF]_n$ (**2**), is successfully prepared. The IR absorptions for bridging and terminal cyanide ligands also occur at 2176 and 2129 cm^{-1}, respectively. The stretching frequencies of the C═O bonds are located at 1653 and 1678 cm^{-1}, which are related to the coordinated and uncoordinated DMF molecules, respectively. Reaction of $Co(NO_3)_2\cdot 6H_2O$ or $Ni(ClO_4)_2\cdot 6H_2O$ with $(Bu_4N)[(Tp)Fe^{III}(CN)_3]$ in methanol and water (v/v = 4:1) yielded the heterobimetallic polymeric complexes, $[(Tp)_2Fe^{II}I_2(CN)_6Co(CH_3OH)_2\cdot 2CH_3OH]_n$ (**3**) and $[(Tp)_2Fe^{III}_2(CN)_6Ni(CH_3OH)_2\cdot 2CH_3OH]_n$ (**4**). Similarly, the IR absorptions for bridging and terminal cyanide ligands occur at 2160 and 2124 cm^{-1} for complex **3** and 2166 and 2123 cm^{-1} for complex **4**, respectively. The stretching absorptions of B−H from the Tp ligand in complexes **1**−**4** are found at 2516, 2519, 2513, and 2514 cm^{-1}, respectively.

Crystal Structures. Selected bond lengths and angles for complexes **1**, **2**, **3**, and **4** are listed in Tables 2−4. The crystal structure for complex **1** has been reported earlier.[7c] It consists of 1D chains of squares. The copper atom is pentacoordinated, with a distorted square-pyramidal geometry. The average intrachain Cu···Fe, Cu···Cu, and Fe···Fe separations are 5.018, 6.782, and 6.782 Å, respectively, whereas the shortest intermolecular Cu···Cu, Cu···Fe, and Fe···Fe distances are 11.100, 8.813, and 8.448 Å, respectively.

Complexes **2** and **1** are isostructural. In **2**, the chain also consists of the basic structure units of the $Fe_2(CN)_4Cu_2$ square with each Cu^{II} shared by two adjacent squares (Figure 1). Within each square, the $[Fe(Tp)(CN)_3]^-$ unit binds two Cu^{II} ions through two of its three cyanide groups. Within the chain, the central Cu(II) ion is pentacoordinated in the form of a slightly distorted square-based pyramid, CuN_4O (Figure 1, top). The bottom plane of pyramid is formed by four nitrogen atoms from the four −CN groups of $[Fe(Tp)(CN)_3]^-$ with the average bond lengths of Cu−N being 1.973(3) Å.

Table 3. Selected Bond Lengths (Å) and Angles (deg) for Complex **3**

Co(2)−N(7)	2.0959(13)	Fe(1)−N(5)	1.9814(12)
Co(2)−N(7)[a]	2.0959(13)	Fe(1)−C(10)	1.9225(15)
Co(2)−N(9)	2.1200(13	Fe(1)−C(11)	1.9131(16)
Co(2)−N(9)[a]	2.1200(13)	Fe(1)−C(12)	1.9182(17)
Co(2)−O(1)	2.0774(13)	C(10)−N(9)[b]	1.1405(19)
Co(2)−O(1)[a]	2.0774(13)	C(11)−N(7)	1.1445(19)
Fe(1)−N(1)	1.9718(13)	C(12)−N(8)	1.143(2)
Fe(1)−N(3)	1.9729(13)	C(10B)−N(9)	1.1405(19)
N(7)−Co(2)−N(9)	91.17(5)	O(1)−Co(2)−N(9)[a]	89.62(6)
N(9)−Co(2)−N(7)[a]	88.83(5)	N(7)−Co(2)−N(7)[a]	180.0
N(7)[a]−Co(2)−N(9)[a]	91.17(5)	N(9)−Co(2)−N(9)[a]	180.00(6)
N(9)[a]−Co(2)−N(7)	88.83(5)	Fe(1)−C(10)−N(9)[b]	175.93(14)
O(1)−Co(2)−O(1)[a]	180.00(4)	Fe(1)−C(11)−N(7)	173.47(14)
O(1)−Co(2)−N(7)	91.34(6)	Fe(1)−C(12)−N(8)	177.82(15)
O(1)−Co(2)−N(9)	90.38(6)	Co(2)−N(7)−C(11)	159.62(13)
O(1)−Co(2)−N(7)[a]	88.66(6)	Co(2)−N(9)−C(10)[b]	167.74(13)

[a] Symmetry operation: $-x+1, -y+1, -z+1$. [b] Symmetry operation: $-x+1, y, -z+1/2$.

Table 4. Selected Bond Lengths (Å) and Angles (deg) for Complex **4**

Ni(1)−N(8)	2.050(3)	Fe(1)−N(5)	1.990(3)
Ni(1)−N(9)[a]	2.033(3)	Fe(1)−C(10)	1.935(3)
Ni(1)−N(8)[c]	2.050(3)	Fe(1)−C(11)	1.911(3)
Ni(1)−N(9)[b]	2.033(3)	Fe(1)−C(12)	1.944(4)
Ni(1)−O(1)	2.064(2)	C(10)−N(7)	1.147(4)
Ni(1)−O(1)[c]	2.064(2)	C(12)−N(8)	1.145(4)
Fe(1)−N(1)	1.981(3)	C(11)−N(9)	1.160(4)
Fe(1)−N(3)	1.974(3)		
N(8)−Ni(1)−N(9)[a]	89.88(10)	O(1)−Ni(1)−N(9)[b]	91.57(10)
N(9)[a]−Ni(1)−N(8)[c]	90.12(10)	N(8)−Ni(1)−N(8)[c]	180.00(13)
N(8)[c]−Ni(1)−N(9)[b]	89.88(10)	N(9)[a]−Ni(1)−N(9)[b]	180.00(18)
N(9)[b]−Ni(1)−N(8)	90.12(10)	Fe(1)−C(10)−N(7)	176.2(3)
O(1)−Ni(1)−O(1)[c]	180.00(16)	Fe(1)−C(11)−N(9)	174.2(3)
O(1)−Ni(1)−N(8)	89.32(10)	Fe(1)−C(12)−N(8)	174.9(3)
O(1)−Ni(1)−N(9)[a]	88.43(10)	Ni(1)−N(8)−C(12)	169.6(3)
O(1)−Ni(1)−N(8)[c]	90.68(10)	Ni(1)[a]−N(9)−C(11)	160.5(3)

[a] Symmetry operation: $-x+2, y, -z+1/2$. [b] Symmetry operation: $x, -y, z-1/2$. [c] Symmetry operation: $-x+2, -y, -z$.

The apical position is occupied by one oxygen atom (O1) of DMF with the bond length of Cu−O being 2.181(3) Å. The bond angles of the apical O(1) with square-based pyramid N and central Cu(II) of N(7)−Cu(1)−O(1), N(16)−Cu(1)−O(1), N(18)[a]−Cu(1)−O(1), and N(9)[b]−Cu(1)−O(1) (the symmetric operation: *a* $x, -y+3/2, z-1/2$; *b* $x, -y+3/2, z+1/2$) are 90.51(14)°, 93.63(14)°, 108.54(13)°, and 95.43(12)°, which deviate from 90°. The coordinated DMF molecules between the neighboring square-based pyramids are opposite each other. $[Fe(Tp)(CN)_3]^-$ is a complex anion with three cyanide ligands in fac arrangement, its symmetry being close to C_{3v}, and the iron atom has a slightly distorted octahedral coordination geometry. The Fe−C (cyano) bond lengths (1.898(5)−1.926(4) Å) are in good agreement with those observed in the low-spin iron (III) complex. The Fe−C−N angles for both terminal (175.6(4)−179.7(4)°) and bridging cyanide (175.2(3)−178.0(4)°) deviate from 180° slightly. Each $[Fe(Tp)(CN)_3]^-$ provides two CN^- groups to coordinate with two Cu(II) ions, leaving one CN^- group free. The pyrazolyl rings of Tp ligands from adjacent chains are dislocated and nonparallel with large separation. The shortest intrachain Fe···Cu, Cu···Cu, and Fe···Fe distances are 4.999, 6.833, and 6.806 Å, respectively, whereas the shortest intermolecular Cu···Cu, Cu···Fe, and Fe···Fe distances are 11.809, 9.120, and 8.768 Å, respectively, which are slightly

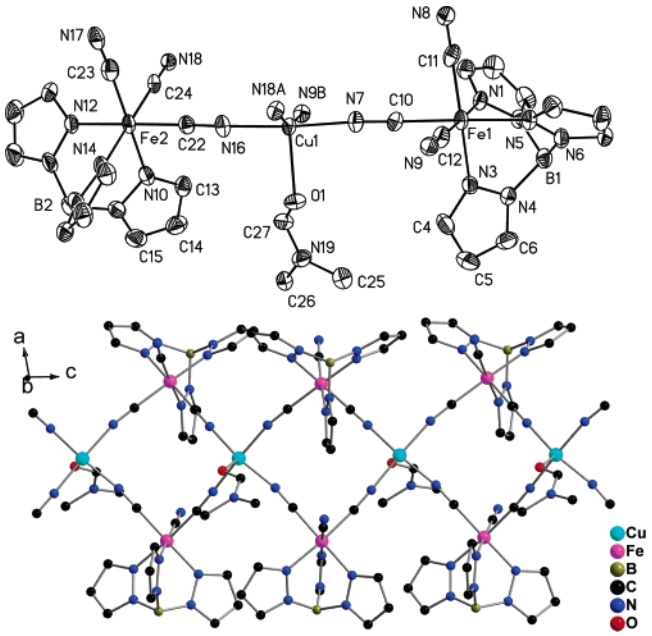

Figure 1. ORTEP view of the crystal structure for complex **2** showing the 30% probability thermal ellipsoid. The hydrogen atoms and solvated DMF molecules are omitted for clarity (top). A perspective view of the 1D squares chain with the atom-labeling scheme (bottom).

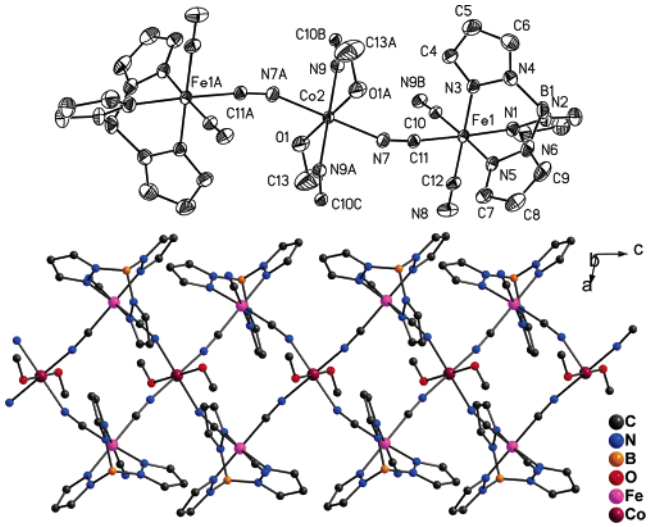

Figure 2. ORTEP view of the crystal structure for complex **3** showing the 30% probability thermal ellipsoid. The hydrogen atoms and solvated methanol molecules are omitted for clarity (top). A perspective view of the 1D squares chain with the atom-labeling scheme (bottom).

larger than the corresponding values in complex **1**. Indeed, the larger solvated molecules (DMF in **2**) show significant effects on molecular packing and thus increase the spacing between neighboring chains. On the basis of the crystallographic data, complex **2** consists of well-isolated 1D $[CuFe_2]_n$ chains with a diameter of ca. 1.4 nm.

The structure of complex **3** is also made up of neutral $Fe_2(CN)_4Co_2$ square units with each Co^{II} shared by two adjacent squares (Figure 2). Within the chain, the central Co(II) ion has a slightly distorted flattening octahedral coordination geometry. The equatorial plane of the flattening octahedron is formed by four nitrogen atoms from the four cyanide groups of $[Fe(Tp)(CN)_3]^-$, and the bond lengths of Co(2)−N(7), Co(2)−N(7)^a, Co(2)−N(9), and Co(2)−N(9)^a

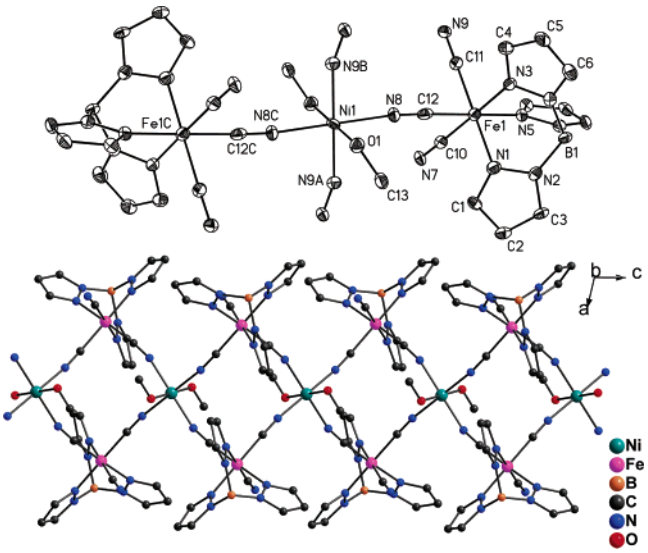

Figure 3. ORTEP view of the crystal structure for complex **4** showing the 30% probability thermal ellipsoid. The hydrogen atoms and solvated methanol molecules are omitted for clarity (top). A perspective view of the 1D squares chain with the atom-labeling scheme (bottom).

are 2.0959(13), 2.0959(13), 2.1200(13), and 2.1200(13) Å, respectively (the symmetric operation: a $-x + 1, -y + 1, -z + 1$). The axial positions are occupied by two oxygen atoms from two methanol molecules with equal bond lengths of Co−O being 2.0774(13) Å. The bond angles of axial O(1) with equatorial plane N and central Co(II) of N(7)−Co(2)−O(1), N(9)−Co(2)−O(1), N(7)^a−Co(2)−O(1), and N(9)^a−Co(2)−O(1) are 91.34(6)°, 93.38(6)°, 88.66(6)°, and 89.62(6)°, which deviate from 90° slightly. The $[Fe(Tp)(CN)_3]^-$ unit binds two Co^{II} ions through two of its three cyanide groups, leaving one CN^- group free. The pyrazolyl rings (C1, C2, C3, N1, and N2) of the Tp ligands from adjacent chains (symmetry: $^1/_2 - x, ^1/_2 - y, -z$) are parallel to each other, and the shorter interchain pyrazolyl−pyrazolyl separation (3.883 Å) indicates that there exist weak interchain $\pi-\pi$ stacking interactions along the a axis (Figure S1 in the Supporting Information). The shortest intrachain Fe···Co, Co···Co, and Fe···Fe distances are 5.036, 6.564, and 6.807 Å, respectively, while the shortest interchain Fe···Co, Co···Co, and Fe···Fe distances are 10.700, 11.505, and 7.913 Å, respectively.

Complex **4** is isostructural to **3** and shows the formation of 1D chains of squares (Figure 3). However, the distortion of complex **4** is slightly larger than that of complex **3**. Within the chain, the central Ni(II) ion has a slightly elongated octahedral coordination geometry. The equatorial plane of elongated octahedron is formed by four nitrogen atoms from the four cyanide groups with the average bond lengths of Ni−N (2.0415 Å). The axial positions are occupied by two oxygen atoms of two methanol molecules with equal bond lengths of Ni−O, 2.064(2) Å. The bond angles of axial O(1) with equatorial plane N and central Ni(II) range from 88.43(10)° to 91.57(10)°, which deviate from 90° slightly. There are weak interchain $\pi-\pi$ interactions from parallel quasi-eclipsed stacking pyrazolyl rings along the a axis, and the shorter distance between them is 3.839 Å. The shortest intrachain Ni···Fe, Fe···Fe, and Ni···Ni distances are 5.002,

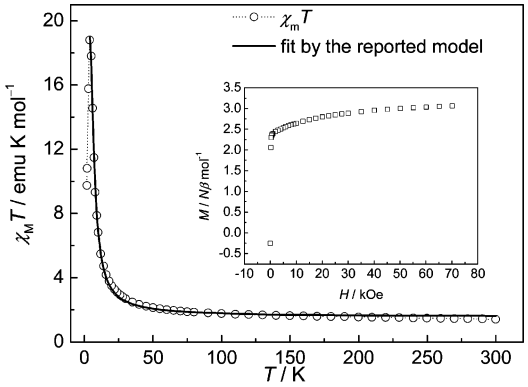

Figure 4. Temperature dependence of magnetic susceptibility in the form of $\chi_M T$ vs T for complex **2**. The solid line is the fitting from 300 to 4 K. Inset: the plot of the field dependence of the magnetization at 1.8 K.

6.717, and 6.547 Å, respectively. The shortest interchain Ni···Fe, Fe···Fe, and Ni···Ni distances are 10.563, 9.216, and 11.369 Å, respectively.

Magnetic Properties. The magnetic properties of complex **1** have been reported, and it exhibits intrachain ferromagnetic coupling and superparamagnetic behavior. The ferromagnetic interaction between the Fe^{III} and Cu^{II} ions is due to the orthogonality of the magnetic orbitals of the two low-spin metal ions. Analysis of ac magnetic susceptibilities gives $\tau_0 = 2.8 \times 10^{-13}$ s and $\Delta/k_B = 112.3$ K, suggesting a thermally activated mechanism. A hysteresis loop is observed at 1.8 K with a coercive field of 120 Oe and remnant magnetization of 0.86 Nβ mol^{-1}. The results from field-cooled magnetization (FCM) and zero-field-cooled magnetization (ZFCM) experiments imply that the blocking temperature is ca. 6 K.

Magnetic measurements for complex **2** were performed on a sample of thin needlelike crystals of random directions in the temperature range of 1.8−300 K (Figure 4). On decreasing temperature, $\chi_M T$ increases gradually from the room-temperature value of 1.621 emu·K·mol^{-1}, which is higher than the spin-only value of 1.125 emu·K·mol^{-1} per Fe_2Cu unit. It reaches 18.80 emu·K·mol^{-1} at 4.0 K and then decreases abruptly until 2 K. This behavior indicates the dominant ferromagnetic interaction and is in agreement with the field dependence of magnetization ($M_S = 3.06$ Nβ, but no hysteresis loop was observed, see the inset in Figure **4**). The ferromagnetic interaction is also ascribed to the orthogonality of the magnetic orbitals as in **1**.

The theoretical expression[16] reported by Drillon et al. for the isolated double chain is

$$\chi = Ng^2\mu^2_B/2kT\{E[4\exp(K^+) + \cosh(K^+) + 1] - 8\cosh(K^+) - \cosh(K^-)\}/\{E[E - 2\cosh(K^+) - 2]\}$$

where $E = 2[\cosh(K^+) + \cosh(K^-) + 2]$, $K^+ = (J_1 + J_2)/2kT$, $K^- = (J_1 - J_2)/2kT$, and J_1 and J_2 are the magnetic interactions within and between the trimers. The best fit to the experimental data between 4 and 300 K gives $J_1 = 14.9(7)$ cm^{-1} (21.5 K), $J_2 = 9.8(9)$ cm^{-1} (14.1 K), and $g = 2.60(2)$, and the agreement factor is 0.9988 (Figure S2).

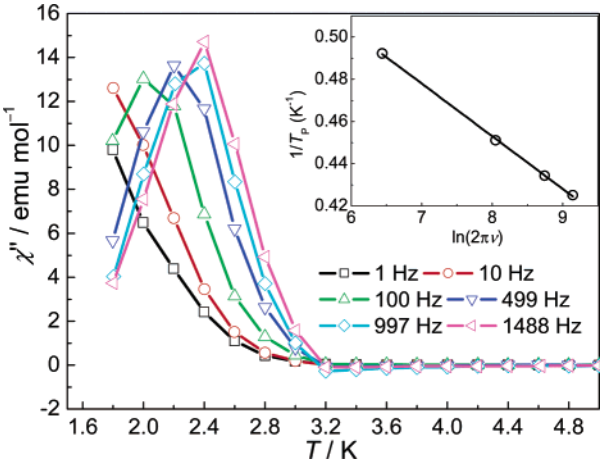

Figure 5. Temperature dependence of the out-of-phase components of the ac susceptibility for **2** in zero applied static field with an oscillating field 5 Oe in the frequency range of 1−1500 Hz. The lines are guides. Inset: the frequency dependence of the ac magnetization was fitted by the Arrhenius law $\tau = \tau_0 \exp(-\Delta E/k_B T)$.

FCM and ZFCM under a field of 100 Oe show the irreversibility below ca. 3 K, which is defined as the blocking temperature (Figure S3 in the Supporting Information).

To probe the dynamics of the magnetization relaxation of **2**, ac magnetic measurements were performed in a 5 Oe ac field oscillating at 1−1500 Hz. Both the in-phase and out-of-phase components go through a maximum (Figure 5 and Figure S4 in the Supporting Information), and they are strongly frequency-dependent below 3 K, precluding a three-dimensional (3D) ordering. The shift of peak temperature (T_P) of χ'' is measured by a parameter $\phi = (\Delta T_P/T_P)/\Delta(\log f) = 0.12$, which is close to a normal value for a superparamagnet.[17] The frequency dependence of T_P of χ'' can be fitted well to the Arrhenius law $\tau = \tau_0 \exp(\Delta/k_B T)$ (inset of Figure 5) with the best set of parameters $\tau_0 = 4.4(7) \times 10^{-12}$ s and $\Delta/k_B = 40.1(6)$ K, suggesting a thermally activated mechanism. The gap is comparable with the expected value $\Delta_{Glauber}/k_B = 2J_{eff'} = 2 \times 21.5 = 43.0$ K based on Glauber's theory.[2b,18]

Complexes **3** and **4** show very different magnetic properties from those of **1** and **2**. The low-temperature magnetic measurements show the metamagnetic behavior in **3** (Figure 6). At applied fields lower than 1 kOe, a maximum of magnetization is observed around 6.0 K, and the maximum disappears for $H > 1.2$ kOe, suggesting a field-induced transition from an antiferromagnetic to a ferromagnetic ground state. This is also confirmed with the field-dependent magnetization as shown in Figure 7. As the field increases, the magnetization first abruptly goes up and keeps a constant of about 0.15 Nβ mol^{-1} from 0.15 to 0.85 kOe, and then shows the second sharp increase above 1 kOe. In the higher field, the magnetization slowly increases reaching 4.8 Nβ mol^{-1} at 70 kOe (Figure S5 in the Supporting Information), corresponding to the expected spontaneous saturation magnetization of 5.0 Nβ mol^{-1} for $CoFe_2$ unit with $S_{Co} = {}^3/_2$

(16) Drillon, M.; Coronado, E.; Belaiche, M.; Carlin, R. L. *J. Appl. Phys.* **1988**, *63*, 3551−3553.
(17) Mydosh, J. A. *Spin Glasses: An Experimental Introduction;* Taylor & Francis: London, 1993.
(18) Glauber, R. J. *J. Math. Phys.* **1963**, *4*, 294−307.

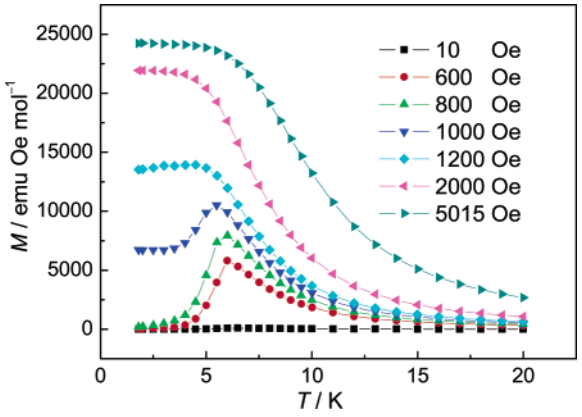

Figure 6. Low-temperature magnetization measurements around the critical field for complex **3**.

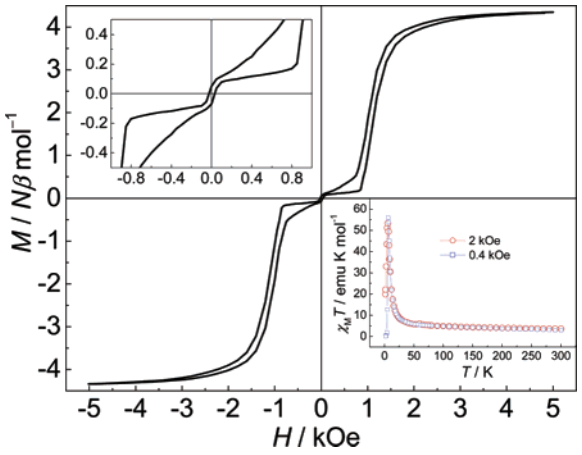

Figure 7. Field dependence of the magnetization for **3** at 1.8 K. Inset: top left, the zoomed $M-H$ plot; lower right, temperature dependences of magnetic susceptibilities in the form of $\chi_M T$ vs T at 0.4 and 2 kOe, respectively.

and $S_{Fe} = {}^1/_2$. The $M-H$ plot shows a typical metamagnetic behavior from spin-canting to ferromagnetic ordering in complex **3**. Taking this into account together with Figure 6, the critical field is around 1 kOe. The canting angle can be roughly estimated to be about 1.7° according to the value of the plateau. When the applied field decreases, the $M-H$ curve is nonreversible and shows a hysteresis loop in both the canting and ferromagnetic regions, where the coercive field and the remnant magnetization are 33 Oe and 0.06 Nβ mol^{-1}, respectively. It is easy to comprehend the metamagnetic properties according to the crystal structure of **3**, i.e., there exists intrachain ferromagnetic coupling and interchain antiferromagnetic interaction (J') by $\pi-\pi$ stacking interactions. And the low critical field suggests that J' is very weak. As shown in Figure 7 (inset, lower right), both $\chi_M T$ at 0.4 and 2 kOe (0.4 kOe < critical field < 2 kOe) increase as the temperature is lowered, indicating the ferromagnetic coupling between the Co^{II} and Fe^{III} ions. However, at 1.8 K and an applied field of 0.4 kOe, the $\chi_M T$ value is close to zero due to the interchain antiferromagnetic interaction below the critical field. The ac magnetizations measured at applied fields of 0 and 2 kOe, respectively, show that both of the antiferromagnetic ordering in the lower field and the ferromagnetic ordering in the higher field occur below about 6 K (Figure S6 in the Supporting Information).

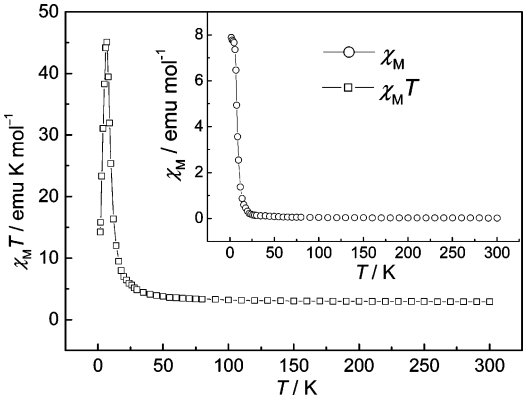

Figure 8. Temperature dependence of magnetic susceptibilities in the forms of χ_M and $\chi_M T$ vs T at 2 kOe for complex **4**. The solid lines are a guide.

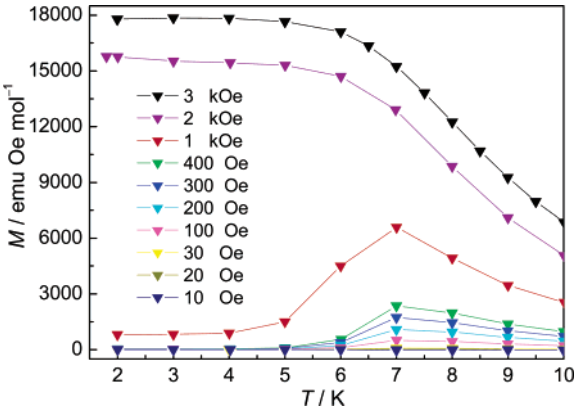

Figure 9. Low-temperature magnetization measurements around the critical field for complex **4**.

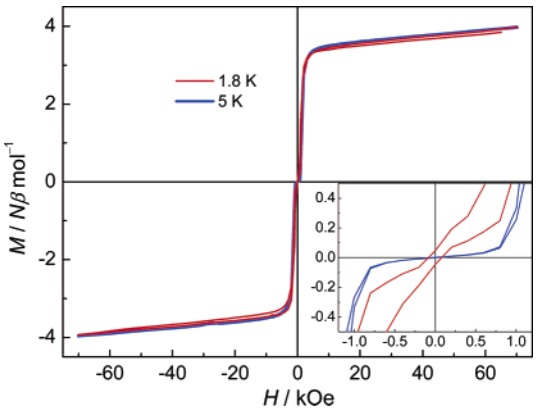

Figure 10. Field dependence of the magnetization for **4** at 1.8 and 5 K, respectively. Inset: the zoomed $M-H$ plot.

Complex **4** exhibits the fairly similar metamagnetic properties to those of **3**. There also exists intrachain ferromagnetic coupling and interchain antiferromagnetic interaction. Figures 8−10 shows the curves of $\chi_M T-T$ (χ_M-T) at an applied field of 2 kOe, $M-T$ at various fields, and $M-H$ at 1.8 and 5 K, respectively. In comparison to **3**, complex **4** has a spin ground state of $S_T = 2$ based on the Fe_2Ni unit. The observed value of $\chi_M T$ at room temperature is 2.9 emu·K·mol^{-1} ($C = 0.125\sum g^2 S_i(S_i + 1) = 1.75$ emu·K·mol^{-1}), and the saturation magnetization at 1.8 K and

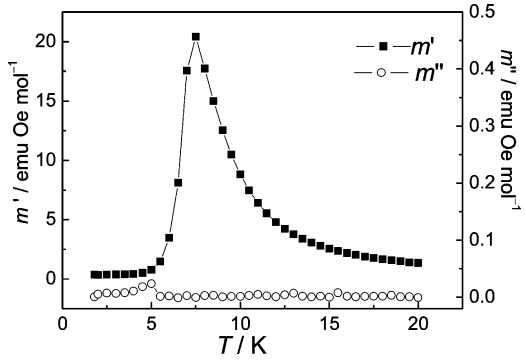

Figure 11. The ac magnetization measurements for complex **4** at $H_{dc} = 0$ Oe, $H_{ac} = 1$ Oe, and $f = 10$ Hz.

70 kOe is 3.96 Nβ mol^{-1} ($gS_T = 4$), respectively. The critical field from the anti- to ferromagnetic ground state is found to be 0.8 kOe, and the coercive field at 1.8 K is 80 Oe, respectively, coming from the $M-H$ plot. The metamagnetic phenomenon is further confirmed by the ac magnetic measurements; when $H_{dc} = 0$, a peak was observed at 7.5 K in the in-phase variable-temperature magnetization, m', but the out-of-phase variable-temperature magnetization, m'', is zero, indicating antiferromagnetic ordering at this temperature (Figure 11).

Conclusion

With the use of the cyanometalate modified with capping organic multidentate ligands as the building block, four 1D heterobimetallic cyano-bridged chains of squares were synthesized. Complexes **1** and **2** show single-chain magnets behavior. The magnetic relaxation behavior should arise from the isolated ferromagnetic nanowires. The blocking temperature is ca. 6 K for complex **1** and ca. 3 K for complex **2**. Complexes **3** and **4** show metamagnetic behavior. The critical field is around 1 kOe for **3** and 0.8 kOe for **4** at 1.8 K, respectively. The differences in magnetic properties among **1**, **2**, **3**, and **4** may result from the different central metal ions and interchain $\pi-\pi$ stacking interactions. Therefore, the effect of interchain $\pi-\pi$ stacking interactions should be kept under consideration for the preparation of single-chain magnets.

Acknowledgment. This work was supported by the National Natural Science Foundation of China, the Major State Basic Research Development Program (Grant No. 2006CB806104), the Program for New Century Excellent Talents in University of China (NCET-04-0469), and Natural Science Foundation of Jiangsu Province (BK2006512). The authors thank Professor Yi-Zhi Li and Dr. Xin-Yi Wang for useful discussions and experimental assistance.

Supporting Information Available: X-ray crystallographic data files in CIF format for complexes **2**−**4** and additional characterization data. This material is available free of charge via the Internet at http://pubs.acs.org.

IC060928D